Methane Detection Through Satellite Imaging: Analyzing and Comparing Methane Concentration in Turkmenistan and Finland

Master's thesis
University of Turku
Physics
2023
B.Sc. Fanni Ristioja
Examiners:
Dr. H. Lindqvist
Dr. M. Irjala
Prof. R. Vainio

The originality of this thesis has been checked in accordance with the University of Turku quality assurance system using Turnitin Originality Check service.

UNIVERSITY OF TURKU
Department of Physics and Astronomy

Ristioja, Fanni Methane Detection Through Satellite Imaging: Analyzing and Comparing Methane Concentration in Turkmenistan and Finland

Master's thesis, 43 pp.
Physics
May 2023

Remote sensing by satellites is a growing field of study and has been applied to environmental research, e.g., in detecting greenhouse gases such as methane. Methane has recently been a major concern for industry due to its global warming potential, which is greater than that of carbon dioxide. This thesis studies methane enhancements in natural gas fields in Southern Turkmenistan using satellite data. These results are then compared to ones from Southern Finland, for which a similar analysis was done in order to see how differences in the areas of interest affect results.

The satellite that was used for this thesis was Sentinel 5 Precursor (S5P) and the instrument that detected methane is called Tropospheric Monitoring Instrument (TROPOMI). S5P dataset is open source and was thus chosen for the analysis. Several plots were done that visualized the data and some additional analysis was done for those plots. Two large methane enhancements were observed in Turkmenistan and they were saved into a GeoJSON file so that the data can be easily distributed and visualised. Some analysis was done using wind data from the time of observation since the two methane enhancements seemed to be spread in certain directions. The wind was not very strong and the wind direction differed from the direction of dispersion; therefore, it was not straightforward to conclude that this caused the observed spread.

There were much poorer quality data available for the area of interest in Finland than in Turkmenistan. The quality of the dataset is determined by the quality attribute (qa), which is usually set to 0.5; pixels with a quality attribute of 0.5 or higher are treated as reliable data points that are not contaminated by, e.g., clouds, and are taken into account. Any pixels with a quality attribute less than 0.5 were discarded. In order to see how much of an effect the quality attribute has, the same analysis was done again for both areas of interest with a quality attribute ≥ 0.25. This was particularly interesting for the area of interest in Finland, which had significantly less data than Turkmenistan when using a higher quality attribute. With a lowered qa the increase in the amount of data points in Finland was significant. This also revealed a new pixel that had higher methane concentration than the others in the area, although it was still a minor increase compared to the enhancements in Turkmenistan. This pixel was further examined, but it did not lead to significant results. However, the experiments showed that a more relaxed qa filtering could prove useful for higher latitude observations.

Keywords: methane, TROPOMI, remote sensing, satellite imaging

Contents

Preface

Detection and monitoring of greenhouse gases is a growing field of study and a global topic that appears in discussions on the current state of our planet. However, there is one gas above all that has drawn scientists' attention during the past few years: methane emission is currently the hot topic of environmental science and its effects on the climate are under increasing examination. Methane is the second most abundant anthropogenic greenhouse gas in the atmosphere after carbon dioxide [1] and its effect on global warming is quantified [2]. Global environment programs and regulations, such as the Paris Agreement, have treated methane as an increasing problem as concentrations continue to grow [3, 4], and have brought new restrictions against it. This is impacting many fields of industry, forcing industrial companies to develop their monitoring systems for methane emissions as well as other greenhouse gases. However, industrial companies also have financial reasons of monitoring methane leaks as they cause economic losses [5].

The satellite industry is a rapidly developing field and when interest in methane's effect on climate change started growing, it began to rapidly introduce detection of methane and other greenhouse gases via remote sensing. Satellite instruments and their algorithms are being constantly developed for better resolution and more precise locating of emission sources.

The European Space Agency (ESA) has launched several Sentinel satellites into space for remote sensing for different fields of study. One of the Sentinel satellites is Sentinel-5 Precursor (S5P) that has an instrument on board which detects methane from space. This instrument is called the Tropospheric Monitoring Instrument (TROPOMI) and it measures methane concentrations using a couple of wavelength bands [6]. S5P has a daily global coverage [6] and the data retrieved from TROPOMI is open source, which makes it suitable for methane study in the purpose of this thesis.

1 Background

The main focus of the first Section is to introduce those components that are relevant to the study in this thesis. Different methods in the field of methane detection are also presented. We will start by introducing the main topic of this thesis, i.e., methane.

1.1 Methane as a greenhouse gas

Methane (CH_4) is the second most abundant anthropogenic greenhouse gas in our atmosphere after carbon dioxide (CO_2). Whilst CO_2 remains in the atmosphere for a long time (over 100 years), methane has a lifetime of approximately 10 years. There is a need to focus on disposing methane from the atmosphere, in addition to reducing and controlling carbon dioxide: whilst CH_4 might be less abundant than CO_2, its global warming potential per unit mass is substantially higher than that of CO_2 [1, 2]. Such a relatively short lifetime in the atmosphere means that if we put our effort into reducing methane emission, we can make a significant difference to methane concentration within the next generation. Reducing methane emissions may have a significant impact on achieving global climate goals [7].

The removal of methane is performed by sinks both in the atmosphere and ground. There is one major sink that reduces methane in the atmosphere and two minor sinks. Oxidation with hydroxyl radical (OH) makes up almost 90 % of the total methane sink, and most methane destruction happens in the troposphere. The photodissociation of tropospheric ozone and water vapor produces OH, which is also the main oxidant of many other tropospheric pollutants. The concentration of OH is the major determinant of the removal rate of atmospheric methane. The two minor sinks are dry soil oxidation and the transport of methane to the stratosphere. [8]

One essential part in understanding the topic is identifying the sources of methane

emission. There are three groups that methane emission can be divided into:

1. Fossil fuel production, such as natural gas, crude oil and coal, which can also be released naturally,

2. Microbial processes in wetlands, landfills, melting of permafrost, livestock and rice cultivation and

3. Biomass burning. [3, 9]

In the above list, there are both anthropogenic, i.e., human made, and natural sources of methane production. Since many methane emission sources are anthropogenic we can make a tangible difference on how much methane is released into the atmosphere. Studying methane emission sources also gives us an opportunity to estimate methane's influence on climate change in the coming years. The largest methane emissions come from so-called ultra-emitters and they can be found to release in excess of 25 tons of CH_4 per hour. In the extreme case, the largest ultra-emitters reach up to several hundred tons per hour and their associated plumes can span hundreds of kilometers from the source. [9]

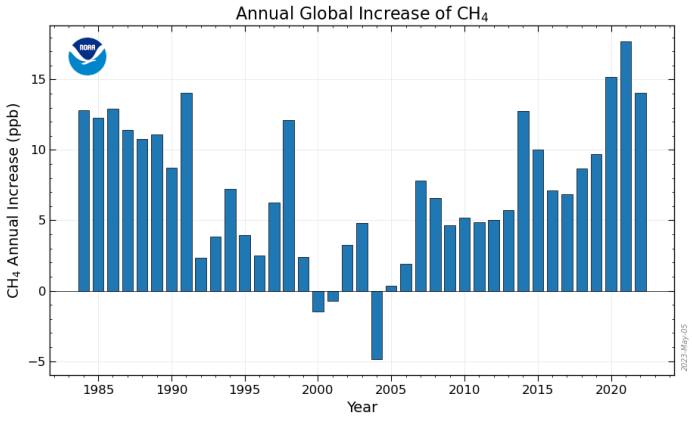

Figure 1. The annual global increase in atmospheric methane [10].

Mean atmospheric methane is measured through a network of different greenhouse gas measuring programs [9]. The annual globally-averaged increase of atmo-

spheric methane is illustrated in Figure 1. The annual growth was at its highest in 2021 and the reason for this is still uncertain. The most recent measurement of monthly globally-averaged mean atmospheric methane abundance is 1921.74 ppb in January 2023, which is 14.3 ppb higher than in January 2022 [10].

1.2 Different ways to detect methane emission

There are several ways to detect methane emission. Most of them are ground-based or aerial, but there are also several satellites orbiting the Earth to detect methane. ground-based methods and some satellite missions are briefly presented below to provide an idea of how many different ways there are to measure methane emissions. Methane is often retrieved as column-average dry-air mole fraction of methane (XCH4) [11]. There is a global network of both ground-based and airborne methods detecting methane [12]. Methane can be measured by the flux method [13] or total column method, in which case the atmospheric transport must be taken into account as methane has a long lifetime in the atmosphere [6].

1.2.1 Ground-based and airborne methods

There are plenty of ground-based detection methods that are either remote sensing or in-situ measurements. Many ground-based detectors are not exclusively measuring methane, but several other gases as well; however, they will only be addressed here in terms of methane detection. Ground-based methods of detecting methane include handheld instruments, fixed sensors and surface mobile (such as vans, bicycles etc.), and airborne methods include drones and planes. [14]

There is a global network of ground-based detectors which consists of high resolution Fourier Transform Spectrometers that record a direct solar spectra in the near-infrared spectral region. This network is called the Total Carbon Column Observing Network (TCCON) and its aim includes improving our understanding of the

carbon cycle and validating the retrievals of satellites. This is possible by providing exact and accurate observations of the mixing ratios of CO_2 and CH_4 for several locations. [14]

Five of the most common ground-based or airborne techniques or devices used in methane detection, of which some are more developed and others are a bit newer, are presented below:

1. Light Detection And Ranging (LiDAR) can be used to map methane concentration from air or different vehicles. LiDAR technology usually has a laser scanning system that has four main hardware components: A laser emitter-receiver scanning unit, differential positioning systems, a highly sensitive inertial measurement unit that is attached to the scanning unit and a computer for controlling the system and storing data.[15]

2. Optical Gas Imaging (OGI) mostly relies on thermal infrared cameras and spectral filtration to visualize methane. OGI is evaluated for methane leak detection by modeling three related physical systems: infrared absorption, imaging properties and leak modeling. [16]

3. Solar Occultation Flux (SOF) is a method that depends on direct sunlight. SOF uses the absorption of direct solar infrared radiation for retrieval of gas concentration. To calculate the total gas leakage from an industrial site, a downwind transect along its plume is conducted and then the integrated concentration is multiplied by the plume wind speed. The SOF instrument consists of a solar tracker, transfer optics and spectrometer. The solar tracker is a mirror device that tracks the Sun and reflects its light into the spectrometer and the signal-to-noise ratio is optimized with optical interference filters. [17]

4. Laser Dispersion Spectroscopy (LDS) is a gas detection technique that uses the phase of light to derive gas concentration so that it is immune to intensity

fluctuations that usually are received at the photodetector. [18]

5. The sniffer method can be applied to different instruments of gas detection. It is used for detecting gas leaks by sucking the sample into the sensor that determines the concentration of gas. In order to capture the gas, the device must be near the source. [19, 20]

1.2.2 Satellite missions

There is a considerable number of satellite missions that have the instrumentation to measure methane from space. Most of them are still on-going, but the oldest have already been decommissioned or lost. Below is a list of some satellite missions and companies or space agencies that detect ground level methane:

1. Scanning Imaging Absorption Spectrometer for Atmospheric Cartography (SCIAMACHY), on board Envisat, launched in 2002 is no longer operating due to the loss of contact to the spacecraft in 2016. SCIAMACHY was the first satellite instrument that was able to measure atmospheric CH_4 from space. [21]

2. Greenhouse Gases Observing Satellite (GOSAT) was launched in 2009 by Japanese Space Agency. GOSAT provides global measurements of both CO_2 and CH_4 and was the first dedicated greenhouse gas detecting mission. It has two instruments on board: The Thermal And Near Infrared Sensor for carbon Observation - Fourier Transform Spectrometer (TANSO-FTS) and the Cloud and Aerosol Imager (TANSO-CAI). [14]

3. The first Greenhouse Gas Satellite (GHGSat) was launched in 2016 and is operated by a Canadian company that goes by the same name. GHGSat has since launched several different commercial satellite missions that detect methane enhancements using high spatial resolution. [22]

4. Tropospheric Monitoring Instrument (TROPOMI) is on board the EU Copernicus Sentinel 5 Precursor (S5P) satellite launched in October 2017 by the European Space Agency (ESA) [12]. S5P is the first Sentinel satellite that measures the composition of the atmosphere [23]. The S5P satellite is expected to have a lifetime of 7 years and it flies in a sun-synchronous orbit at 824 km altitude [21].

5. Greenhouse Gases Observing Satellite-2 (GOSAT-2) was launched in 2018 and it is the follower of GOSAT. GOSAT-2 is very similar to its precursor with the same mission but with updated instruments on board including improved cloud detection capability. [24]

6. Finnish company called KuvaSpace is using nanosatellites to track carbon emissions that include methane. There are currently three active satellites that use hyperspectral camera technology and AI-based analytics. These provide compact satellites with high performance. [25]

There are also some new satellite missions to be launched that are worth mentioning:

1. Methane Alert and Response System (MARS), launched by the United Nations Environment Programme, is going to be the first publicly available global system that works with other satellites to detect major methane plumes and hot spots. [26]

2. MethaneSAT LLC will launch a methane concentration measuring satellite in the end of 2023. MethaneSAT is going to be the most advanced satellite in the field so far and it will be measuring methane emission across the globe. [27]

3. Copernicus Anthropogenic Carbon Dioxide Monitoring (CO2M) is a mission

operated by ESA and will be launched in 2026. It will contain three instruments that also provide methane observations and retrieval. [28]

4. Methane Remote Sensing Lidar Mission (MERLIN) is a mini-satellite mission that is due to be launched in 2028. The instrument on board is an Integrated Path Differential-Absorption Lidar (IPDA LIDAR), which is using laser light to determine columns of methane in the atmosphere. The IPDA LIDAR has a high degree of accuracy and precision of spatial and temporal gradients of the determined columns. [28]

Multi-spectral instruments have high spatial resolution for methane detection which ensures an improvement in the accuracy of identifying methane emission sources. High spatial resolution enables more precise quantification of emission rates using retrieval algorithms that estimate methane concentration enhancements. [29]

1.3 TROPOMI

In what follows, we will give a more detailed description of the instrument used in this study: The push-broom imaging spectrometer called the Tropospheric Monitoring Instrument (TROPOMI) that is onboard Sentinel-5 Precursor (S5P). A push-broom imaging spectrometer is an instrument that scans the Earth while the satellite is moving. TROPOMI enables real-time CH_4 monitoring from space and combines air quality and greenhouse gas monitoring with a daily global coverage [30]. It has a swath of 2600 km [31] and its ground-pixel varies from $3.5 \times 5.5\,\mathrm{km}^2$ in near infrared (NIR) bands, to $5.5 \times 7\,\mathrm{km}^2$ in short wavelength infrared (SWIR) bands [11]. Before August 2019 the resolution was a bit lower than nowadays and it has been updated by reducing the integration time of observation [32]. Figure 2 shows the measurement principle of TROPOMI, where the different dimensions are shown.

TROPOMI has two spectrometer modules: the first one has ultraviolet (UV), visible (VIS) and near infrared (NIR) spectral channels and the second one has the

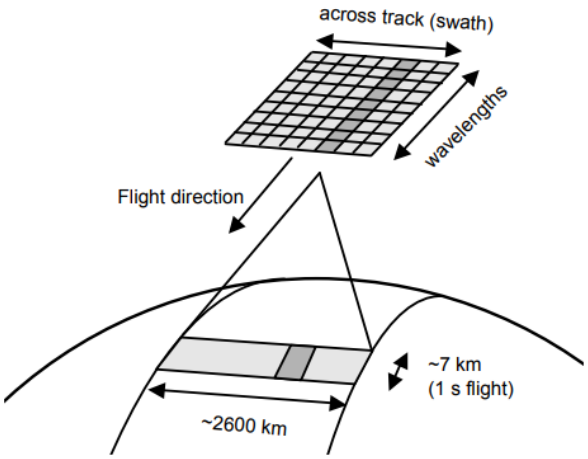

Figure 2. The observation principle of TROPOMI [23].

short wavelength infrared (SWIR) channel. In wavelengths, TROPOMI's spectral ranges are $279 - 320\,\text{nm}$, $310 - 495\,\text{nm}$, $675 - 775\,\text{nm}$ and $2305 - 2385\,\text{nm}$ [21]. A visualization of the electromagnetic spectrum is shown in Figure 3, where NIR and SWIR wavelengths can be seen more closely.

2 Theoretical Aspects

Theoretical aspects of TROPOMI's retrieval algorithm such as the retrieval model, are covered in this Section as well as the algorithm itself. The physics behind detecting and retrieving methane using TROPOMI are also explained in this section.

2.1 Retrieval of methane from TROPOMI

TROPOMI measures reflected solar radiation, from which the corresponding value of methane is retrieved. Retrieval is based on measuring the absorption bands caused by atmospheric CH_4 molecules. These measurements are disrupted by aerosols and clouds in the atmosphere. The method uses Oxygen A-band and absorption bands of the target absorber, which, in this case, is methane, in the SWIR spectral range

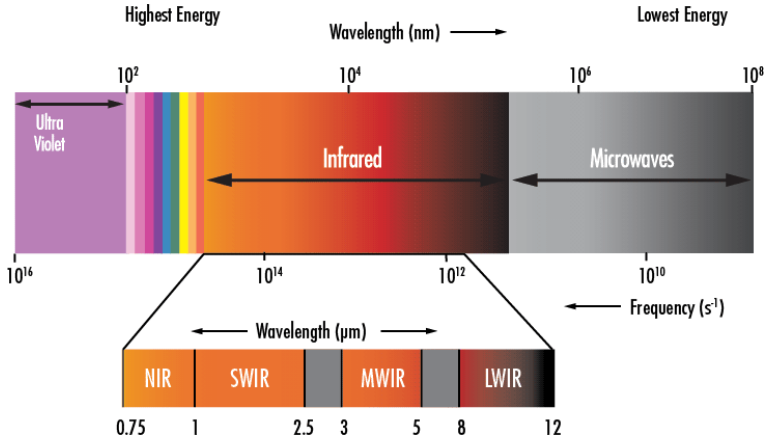

Figure 3. Illustration on where NIR and SWIR channels lie on the spectral range [33].

[6]. TROPOMI's operational CH_4 retrieval algorithm is based on the RemoTeC algorithm, which simultaneously retrieves the amount of CH_4 in the atmosphere and the physical scattering properties of the atmosphere. The RemoTeC algorithm is inspected more closely in Section 2.1.1. It was first used for retrieving CO_2 and CH_4 from GOSAT observations [21], and so the properties and physics of TROPOMI are strongly based on the previous satellite missions of SCIAMACHY and GOSAT [6]. Important features of the retrieval algorithm are its accuracy and speed, which allows for the processing of the large amount of data provided by the satellite [21].

The goal of the RemoTeC algorithm is to infer a state vector that contains all wanted parameters from the radiance measurements. It works on radiance measurements in the SWIR and NIR spectral bands [34]. However, the NIR band has problems with straylight, which is currently dealt with by calibration efforts to improve the straylight correction [30]. RemoTeC retrieves CH_4 as column-average dry-air mole fraction (XCH_4) [11]. XCH_4 will be used later in this thesis when addressing the retrieved data and CH_4 will be used when addressing methane in general.

TROPOMI dataset has some issues because of the large pixel size, resulting in gaps in observations. Non-ideal weather and environmental conditions, such as high humidity, clouds and very dark or bright surfaces cause difficulties in the retrieval

of methane, leading to missing data over some areas [31]. To get reliable data and minimize the effect of non-ideal conditions a quality assurance value, which will later be referred to as quality attribute or qa, is presented in retrieving methane. This value is usually set to 0.5 based on a recommendation from the algorithm developers, and data points with a quality attribute below this value are discarded. [23]

A major problem of detecting methane from space is scattering due to clouds and aerosol. This scattering modifies the lightpath and cause retrieval errors if not properly accounted for. This is a general problem for all satellites that detect methane in the short wavelength infrared region. [21]

There is some residual in TROPOMI data caused by clouds. Optically thick clouds can be filtered out quite efficiently, but optically thin scatterers might cause some trouble. These thin clouds can be hard to detect and can still significantly modify the light path of the observed back-scattered sunlight, causing under- or overestimation of the true methane column. This can be taken into account in the retrieval method and by using the method that RemoTeC algorithm uses, called the full-physics method. The algorithm takes into account the scattering-induced light-path modification by simultaneously considering the atmospheric CH_4 concentration and physical scattering properties of the atmosphere [6]. The full-physics method is not the only way to retrieve methane and, depending on the instrument, a simpler method called the proxy method can be used. Whilst the full-physics method can consider scattering, the proxy method cannot. The proxy method assumes that scattering effects will cancel out in the ratio of CH_4 and CO_2 columns and that scattering is ignored in the retrieval process. TROPOMI does not have a suitable lightpath proxy for methane at the SWIR band and thus the full-physics method is required. [30]

TROPOMI is not generally able to measure methane enhancement above water due to its dark surface. This is the reason why water causes missing values in the

data and can lead to errors in retrieving a pixel. The only exception are parts of an ocean that are close to the equator; there surface glint enables measurements because the Sun reflects from the surface in the specular reflection angle that is observed by TROPOMI. The pixel is retrieved if the sun glint angle is suitable. [6]

Before getting to the actual part of data analysis, the models in the retrieval algorithm are inspected more closely and an overview of the processing per ground pixel, i.e., how the dataset is retrieved, is given. The forward model of the retrieval algorithm is also explained in order to better understand the algorithm's process. The following introduction in Sections 2.1.1 and 2.1.2 is based on the Algorithm Theoretical Baseline Document for Sentinel-5 Precursor Methane Retrieval by O. Hasekamp *et al.* [6].

2.1.1 Retrieval forward model and inversion

The retrieval forward model simulates the physical processes that affect light passing through the atmosphere. The measurement vector $\boldsymbol{y}$ for a given model atmosphere is simulated by the retrieval forward model $\boldsymbol{F}$, which is defined by the state vector $\boldsymbol{x}$ and the ancillary parameter vector $\boldsymbol{b}$. $\boldsymbol{y}$ contains the measured radiances at NIR and SWIR channels and is given by

$$\boldsymbol{y} = \boldsymbol{f}(\boldsymbol{x}, \boldsymbol{b}) + \boldsymbol{e}_y, \tag{1}$$

where $\boldsymbol{e}_y$ is the measurement noise vector and $\boldsymbol{f}$ is the true forward model. In order to approximate the true forward model $\boldsymbol{f}$, the retrieval forward model $\boldsymbol{F}$ is used. The measurement vector can be expressed as

$$\boldsymbol{y} = \boldsymbol{F}(\boldsymbol{x}, \boldsymbol{b}) + \boldsymbol{e}_y + \boldsymbol{e}_F, \tag{2}$$

where $\boldsymbol{e}_F$ is the forward model error vector. The retrieval forward model is a simplified version of the true forward model and it can use a look-up table where precalculated radiance spectra are saved in order to solve for the atmospheric methane

concentration for the observed radiance spectra. The simulated radiance for a given spectral pixel i, $I_{\mathrm{conv},i}$, is given by

$$I_{\mathrm{conv},i} = \int_{\lambda_{min}}^{\lambda_{max}} I(\lambda)\, S_i(\lambda)\, d\lambda \tag{3}$$

in which $I(\lambda)$ is the intensity modeled by the radiative transfer code, and $S_i(\lambda)$ is the Instrument Spectral Response Function (ISRF) for spectral pixel i, for a given wavelength λ. The ISRF for all the spectral channels is stored in a matrix, which is then used to perform the convolution. In discretized form, the convolution can be written with the ISRF as

$$\boldsymbol{I}_{\mathrm{conv}} = \boldsymbol{S}\, \boldsymbol{I}_{\mathrm{fine}} \tag{4}$$

in which $\boldsymbol{I}_{\mathrm{conv}}$ is a vector that contains the modeled intensity for all spectral pixels, $\boldsymbol{S}$ is a matrix that contains the ISRF for all of the spectral pixels and $\boldsymbol{I}_{\mathrm{fine}}$ is the modeled intensity spectrum at high spectral resolution.

The retrieval forward model uses a model atmosphere composed of 36 homogeneous vertical layers; these layers are defined at specific pressure intervals. The largest level of pressure is defined by the surface pressure.

After applying the forward model, an inverse method is used to optimize the state vector $\boldsymbol{x}$ with respect to the measurements $\boldsymbol{y}$. Usually the measurements contain insufficient information for retrieving the state vector elements independently so the inversion is ill-posed. Thus, the inversion is based on a common regularization scheme. [6]

2.1.2 Overview of processing per ground pixel

To get a general idea of how the retrieval algorithm of TROPOMI works Figure 4 summarises the processing per ground pixel. The algorithm uses pre-processed input data for each of the ground pixels. The left side of Figure 4 is where the

algorithm starts by performing a priori filtering that is based on cloud data usually provided by the Visible Infrared Imaging Radiometer Suite (VIIRS) satellite instrument. Fast Retrieval Scheme for Clouds from the Oxygen A-band algorithm (FRESCO) provides data of apparent surface pressure that is retrieved with no scattering of aerosols or clouds and Softwave Infrared Carbon Monoxide Retrieval algorithm (SICOR) is the carbon monoxide (CO) retrieval algorithm. The retrieval is not performed if there is too much cloud contamination or if there is too large variation in cirrus reflectance between the spatial ground pixels in NIR and SWIR bands.

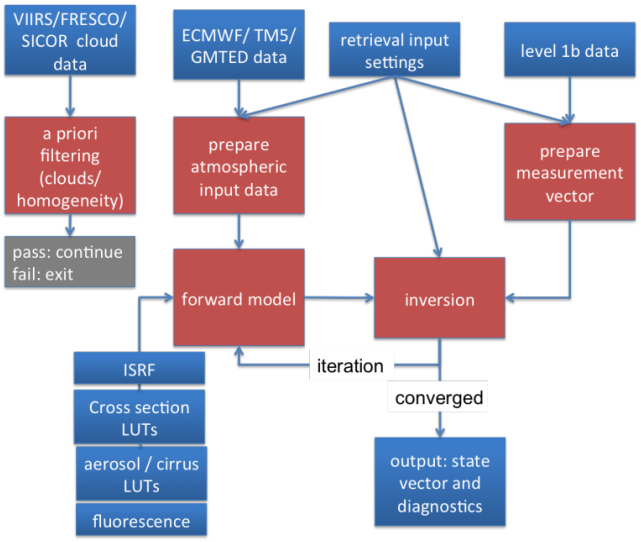

Figure 4. Overview of the processing of per ground pixel by RemoTeC algorithm [6].

If a priori filtering is successful, the algorithm moves on to preparing atmospheric input data. These data are used in retrieval, i.e., the dataset is prepared for interpolation to the vertical grid of the retrieval forward model and also for filling the values of the initial state vector. These data are usually retrieved from the European Center for Medium Range Weather Forecast (ECMWF).

The third step of the process is the iterative scheme. Now the forward model calculation is performed for the first guess vector. Inversion is performed for the

state vector and it is based on the forward model calculation, the measurement vector and prior information. This step is performed until convergence is reached. The final retrieved data are validated and made available for further analysis and research.

2.2 Emission estimation

Methane emission is not estimated in this thesis, but a brief introduction to emission estimation is given in order to separate the observation of methane concentration and emission estimation.

One thing worth pointing out, that does not necessarily affect only TROPOMI data but rather is a general issue of all methane retrieving satellites, is that the difficulty of data analysis of methane from satellite data lies with the background. The satellite measures all of the atmosphere and because the atmospheric lifetime of methane is long, which means that there can be methane that actually originated from another source than the area under consideration. This means that one cannot just point out an assumed source and say how much methane it produces, as the wind can carry methane even long distances and distort the emission estimation. While background reduction gives some information about the actual emission source, calculating the exact amount of emission would require more advanced and complicated methods that are not used in this thesis. The goal of the methods is to quantify the emission of the source.

A couple of methods are briefly presented that can be applied to satellite data. A very common method is the mass balance method, which applies the local wind speed to the observed methane enhancement. This model assumes that the mass is moving due to the wind but it does not take into account some factors, which results in an underestimate of the emissions. [35]

There are also methods using a Gaussian approach, that is using Gaussian statis-

tics for modeling the methane dispersion from a point source. The Gaussian integral method can be used to estimate daily methane emission and it includes coordinate transformation, gridding the data and a definition of mean wind. Gridding the data means that the irregularly spaced satellite data are interpolated into a regular grid. After this the daily emission rate is estimated by calculating the fluxes of a vector field through cross sections that are perpendicular to wind direction. The final daily flux is estimated as the average of all the fluxes through the cross sections. [1]

Another Gaussian model is called the Gaussian plume inversion, which is used to model enhancements in methane concentration downwind of a point source. This method uses Gaussian inversion, which requires a Gaussian plume morphology that is suited for the inversion, and calculates the flux density at all points across a vertical plane perpendicular to the mean wind direction. This is related to the mass balance method previously described. [36]

3 Data and methods

S5P Level 2 (L2) bias-corrected data product produced by the European Space Agency (ESA) is used for data analysis in this thesis [30, 34]. L2 data refers to the geophysical data products that are derived from the data that TROPOMI collects [23]. The bias correction of XCH_4 is performed in order to improve the accuracy of the product [23]. The analysis is done for two different areas of interest: one with a high concentration of methane enhancement and one with lower. These two areas are very different and were chosen in order to show the difference in analysing such geographically diverse areas and the change in the quality of the satellite data on a higher latitude. The first area is in South-East Turkmenistan and has two large natural gas fields with a large amount of methane emission and good quality data [1]. The area that was chosen in Finland is a part of large gas transmission network that consist of interconnected natural gas pipelines [37].

A less optimal area was chosen so that it could be shown how much the features of the area affect the results we get and how important it is to choose the right instrument for the area of interest. For example TROPOMI has less data from the northern parts of the globe and so the quality of the analysis in those parts is not as good when compared to more southern locations. As clouds can contaminate the pixels, so that they cannot be used, there is less data in more cloudy areas with changing seasons. The changing seasons result in less radiation, especially in the northern parts of the globe, so satellite measurements are not possible for the whole year. For these reasons TROPOMI is not good for measuring methane enhancement in Finland, for example, where there is expected to be significantly less enhancement in comparison to the area of interest in Turkmenistan. Figures 5 and 6 show the areas of interest.

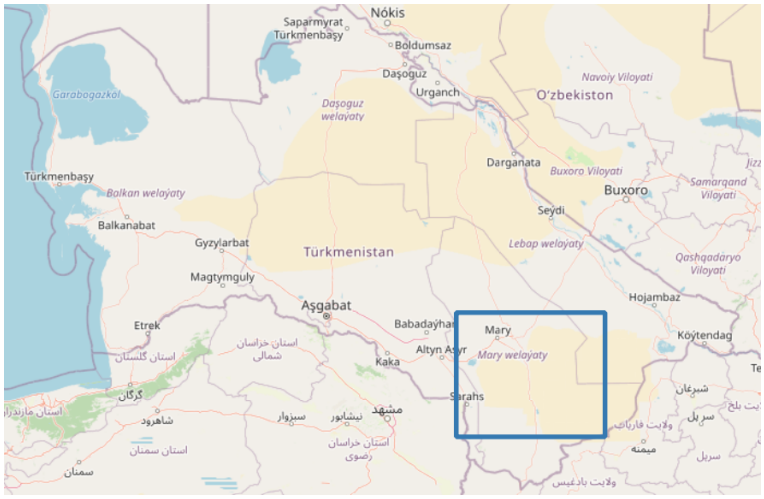

Figure 5. The area of interest in Turkmenistan.

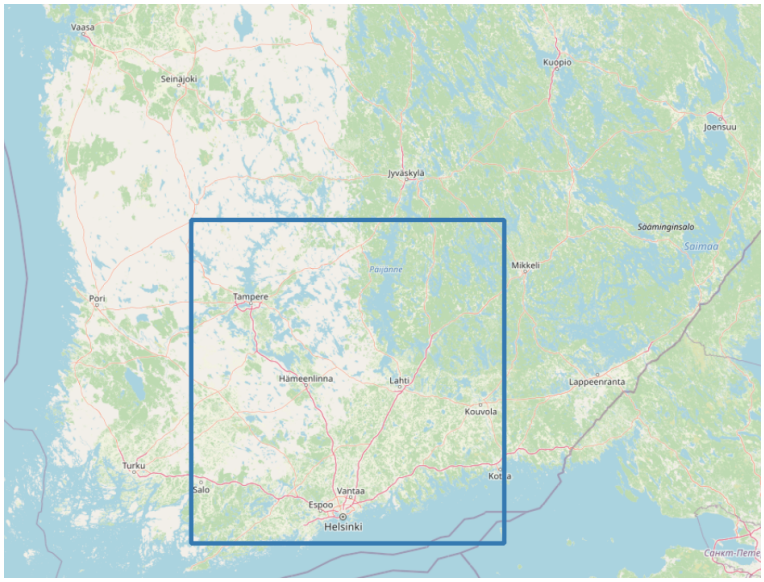

Figure 6. The area of interest in Finland.

After the analysis the found enhancements were saved into a GeoJSON file so that it is easy to plot them for example on top of Google Maps to see where the enhancements are located and what the areas look like.

3.1 Retrievals from TROPOMI

The very first thing to do was to prepare a clear plot of the satellite data, which was done for data from 31 August 2021. Methane values were found to be between 1800 ppb and 2000 ppb, so the dataset was scaled to fit that range to get a plot where methane is actually seen. To get a better idea of the actual enhancement, the atmospheric methane background was reduced by calculating the median of all of the values and subtracting it.

Next, a histogram was plotted to show the distribution of the values and to see the variety in methane concentration within the area. The median of methane values was added to the histogram as a vertical line in order to see where the background settled. Since the background is often the main source in satellite imaging of methane, the distribution is expected to be mostly Gaussian with only methane

enhancements differing from that.

For the purpose of later comparison the percentage of so called good pixels was calculated. Good pixel values were defined to be those with a quality attribute 0.5 or higher. The proportion of good pixels from June 2021 to August 2021 is calculated, so that they could be compared to the proportion of good pixels from the same period measured in Finland. The three summer months were chosen so that the best possible results could be compared and because methane is usually best detected during summer. The proportion was calculated by simply taking the ratio of the valid data points and the total points in the area.

For the aforementioned analysis the good pixels were defined by setting the quality attribute to 0.5 to get data for inspection, but to show how quality attribute affects the retrieved data, it was next reduced by half to 0.25. All of the steps described before were done again, but with this lower quality attribute.

The first challenge for getting started with the data analysis in Finland was finding any data at all. The values were set between 1800-1900 ppb as it was expected that the values would be lower in Finland than they were in Turkmenistan, but it took a good number of dates to find one with more than a couple of pixels. The one with the most data was dated 17 July 2021; this was plotted the same way as a similar one from Turkmenistan and after the reduction of background, the scale was set the same so that the comparison of the two figures would be easier.

A histogram of XCH_4 values was also made for the area in Finland. In this case most of the values in the histogram belong to the background with slight variation coming from contamination and the fact that the background is not always constant. This histogram was combined with the similar one for Turkmenistan and this final plot is presented as the result.

The total amount of pixels over the three months was also calculated for Finland. This was done for June, July and August 2021 and the distribution was plotted in

the same figure as the Turkmenistan distribution.

The quality attribute was again set to 0.25 and the same steps were repeated for the area of interest in Finland. Lowering the quality attribute for the data in Finland had a more pronounced effect on the results than it had for the area in Turkmenistan. The weather situation at the time of observations was obtained in order to see if there were any clouds during the observations that could affect the reliability of the increased data. This was done using Worldview [38], an online, publicly available service operated by the National Aeronautics and Space Administration (NASA). These were done only for Finland because the results in Turkmenistan did not significantly change the outcome of the previous analysis with higher quality attribute, whereas in Finland there was much more data to consider with a lower quality attribute.

3.2 Wind data

When the enhancements in the Turkmenistan area were further inspected, it seemed like there could be some spreading of the plumes caused by wind. To examine this further, some data analysis was done using wind data provided by the Copernicus Climate Data Store [39]. The dataset used in this analysis is collected by the European Centre for Medium-Range Weather Forecasts (ECMWF). This dataset was already processed and so could be directly plotted with the wind direction and strength shown in vector format. The wind dataset is given in u- and v-components from which the data with height of 10 meters was chosen for the analysis. The u- and v-components are the vector components of Eastward and Northward wind.

The data that were used was from 31 August 2021, which is the day of the TROPOMI observations from before. The average wind speed from that day was calculated and then plotted on top of the enhancement map of Turkmenistan, so that the wind direction could be easily compared to the directions of the enhancement

plumes. There are wind data from each hour of the day but it is limited to a couple of hours before and during the overflight time. As TROPOMI passes the area between 8.30 UTC and 9.30 UTC, the hours taken into account are from 6.00 UTC to 10.00 UTC.

3.3 Statistical analysis

The skewness of the XCH_4 histograms was calculated to inspect how the values are distributed more closely. Skewness is a statistical method of calculating the asymmetry of the distribution. A negative skewness value means that the tail on the left side of the distribution is longer than on the right side. Conversely, the right side is longer if skewness value is positive and if the value is zero then the tails are same length. Skewness is quantified by the Fisher-Pearson coefficient:

$$g_1 = \frac{m_3}{m_2^{3/2}}, \tag{5}$$

where

$$m_i = \frac{1}{N}\sum_{n=1}^{N}(x[n] - \overline{x})^i, \tag{6}$$

is the biased sample ith central moment, N is the sample size and $\overline{x}$ is the sample mean. [40]

3.4 GeoJSON processing

For saving the useful information about methane enhancements in a more convenient way, the pixels that have a higher methane enhancement are saved in the Geographical JavaScript Object Notation (GeoJSON) format. This particular format was chosen so that the emission sources could be easily visualised later whilst being saved in a compact format where there would be all the necessary information easily available. GeoJSON files are written similarly to JSON files. Whilst a JSON is a file mainly used in transferring data and the information is text format,

GeoJSON is a file where different geometries can be saved using coordinates. Thus, a GeoJSON file includes geographical data in a compact size with some information about the data. In this case the information includes only the amount of methane the area contains. GeoJSON is a format understood by web pages so it is also a very useful and easy way to represent methane enhancement.

The code that was written for saving the enhancements into GeoJSON mainly consists of different functions that have their own task. The steps taken to accomplish the GeoJSON file are as follows:

First it is important to note that only those pixels with high enough values were saved into the file to achieve a compact and small enough file. The threshold was determined by the 0.98 quantile and thus only pixels with methane values higher than 1950 ppb were taken into account. Next the area is defined, which is the same as was under consideration before, and the coordinate reference system is defined. Now we take each individual element of the data array and turn it into a GeoJSON format, with the GeoJSON containing the geometry of the coordinates of each individual pixel of the array.

At this point we have a GeoJSON file that has a lot of geometries and is still quite a large file, so it is not as efficient as is aimed for. This can be compressed by combining the neighbouring geometries that have the same values into one. After this compression is done for all of the geometries in the file, the result is the original raster file turned into GeoJSON with reasonable size.

4 Results

The results of the data analysis are collectively shown in this Section.

4.1 Methane concentration in Turkmenistan

First, Figure 7 shows methane concentration in Turkmenistan when the quality attribute is set to 0.5, so that those values that have qa value 0.5 or higher are taken into account. In Figure 7 one can see the coordinates of the observed area and the abundance of ΔXCH_4 are shown with a color bar that has values in the range from -20 to $+80$ ppb due to the background reduction. Figure 7 clearly shows two sources of methane enhancements observed at that time. The reason why this specific date was chosen, is that it simply produced the best Figure that showed the enhancements clearly and they could be easily separated from each other. These enhancements are caused by large natural gas fields in the South-Eastern part of Turkmenistan and their location is better seen in Figure 9, which shows the methane enhancements plotted on a map of the area in GeoJSON format, which will be addressed later. Figure 8 shows similar plot as Figure 7, but with quality attribute ≥ 0.25.

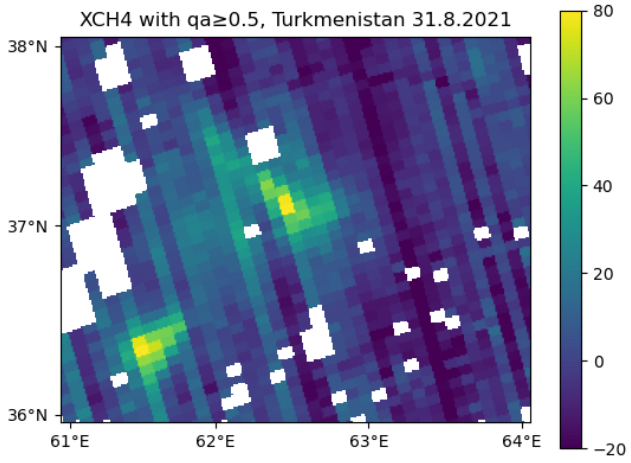

Figure 7. Methane enhancement in Turkmenistan with reduced background. The color bar shows the abundance ΔXCH_4 in parts per billion (ppb). White areas represent either those pixels that have been contaminated or those that have the quality attribute less than 0.5.

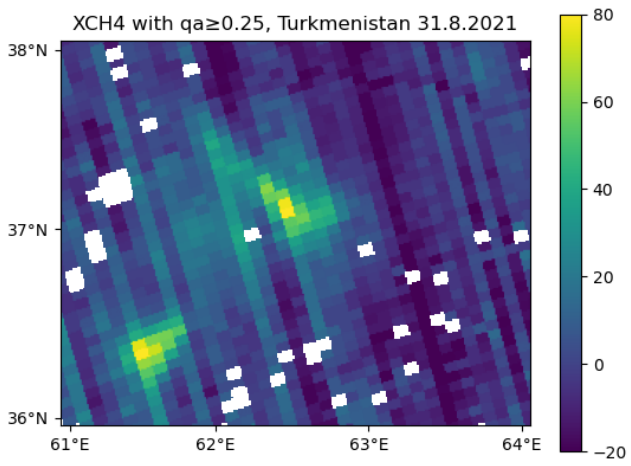

Figure 8. Methane enhancement in Turkmenistan with reduced background and qa$\geq$ 0.25. The color bar shows the abundance ΔXCH_4 in parts per billion (ppb). White areas represent either those pixels that have been contaminated or those that have the quality attribute ≥ 0.25.

Figure 9 shows the GeoJSON file that was constructed for the methane enhancements in Turkmenistan. The pixels in the 0.98 quantile are saved into the file which means that the values are higher than 1950 ppb. This is set so that only those data points that have a sufficiently large methane concentration are saved into the file and only these methane enhancements would be further observed in order to determine the emission of the source. Overall, the saved GeoJSON file has two clear methane enhancements and some individual pixels that are separate from the larger ones. Notably this whole process can be done automatically: When a new image is uploaded we run this analysis pipeline and output the areas with the highest methane concentrations.

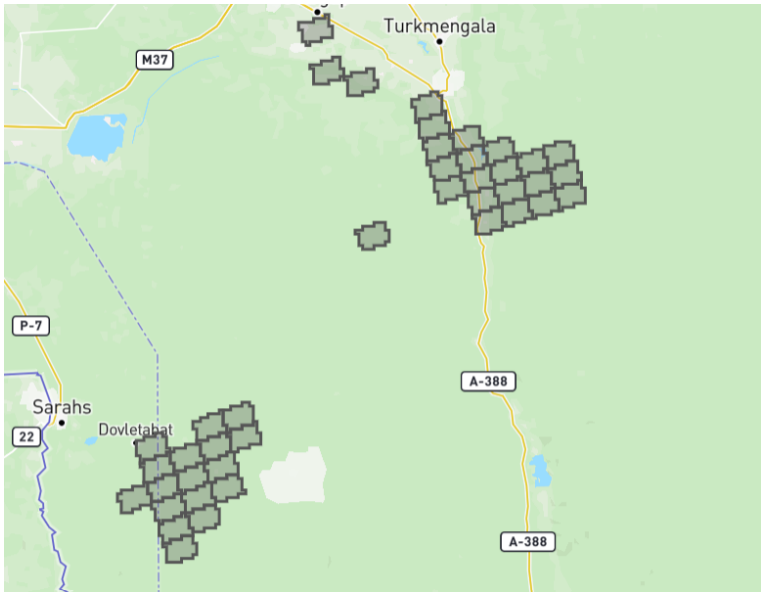

Figure 9. Figure that shows the GeoJSON transmitted into a map application website. The values saved into GeoJSON are higher than 1950 ppb.

The wind data plotted for 31 August 2021 is shown in Figure 10 and it can be further inspected to get some idea about the spreading of the plumes. The wind is shown as vectors in Figure 10 and the size of the vector describes the speed of the wind: the longer the vector, the stronger the wind. If the Western one of the two methane enhancement is first inspected it is noted that there is minor wind to the southern direction. The wind on the eastern source is stronger and in the South-East direction.

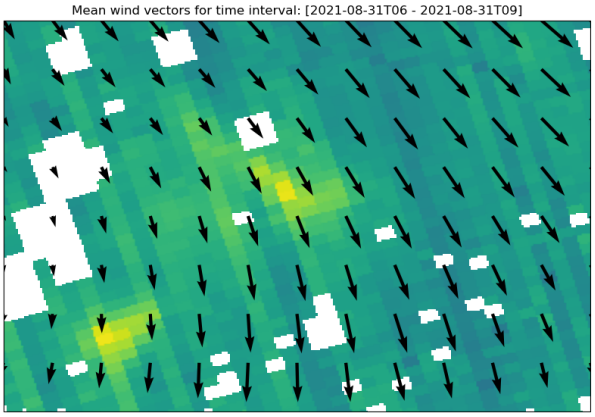

Figure 10. Plot of wind as vectors a couple of hours before and during the time that TROPOMI passes the area of interest.

4.2 Methane concentration in Finland

Methane concentration with background reduction in Finland and both of the quality attributes are presented in Figures 11 and 12, which are presented at the same scale as the similar plots of Turkmenistan. There are a lot more missing pixels in Figure 11 than in Figure 12, causing large white areas in the plot and making it difficult to perform further analysis on the area.

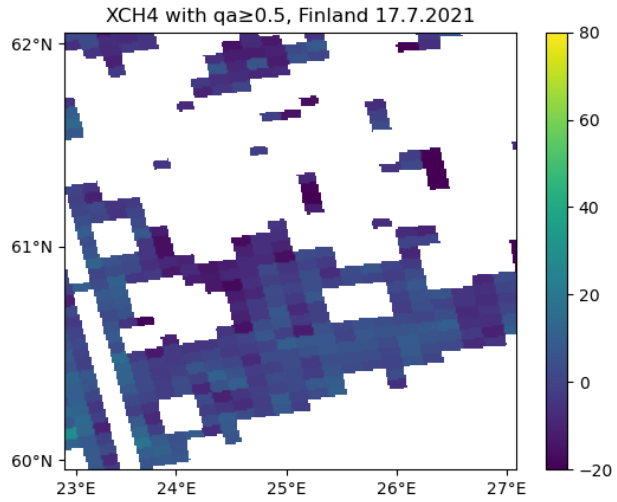

Figure 11. Methane enhancement in Finland with reduced background. The color bar on the right shows the abundance ΔXCH_4 in parts per billion (ppb). White areas represent either those pixels that have been contaminated or those that have the qa-value less than 0.5.

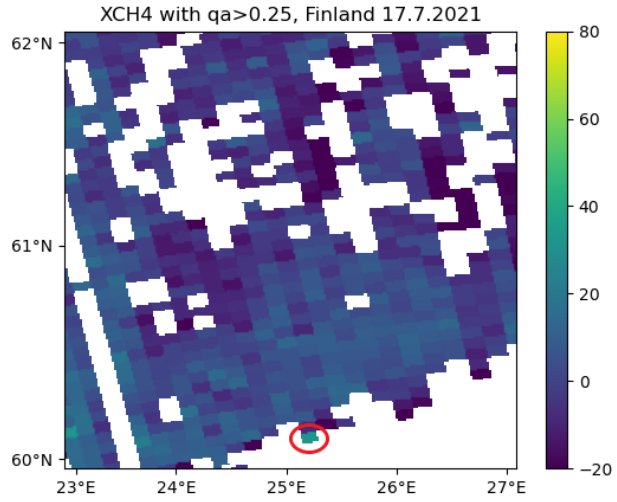

Figure 12. Methane enhancement in Finland with reduced background and qa $\geq$ 0.25. The color bar on the right shows the abundance ΔXCH_4 in parts per billion (ppb). White areas represent either those pixels that have qa less than 0.25. The pixel that is marked in red is one that was not seen before and has an increased methane concentration.

The overall cloud cover in Southern Finland at the area of interest during the time of observation was checked in order to see whether the new pixels that were released by lowering the quality attribute might be contaminated by clouds. The cloud cover is shown in Figure 13 and it can be seen that there is none during the time of observation.

Figure 13. Cloud cover of the area of interest in Finland on 17 July 2021 by Earth Observing System Data and Information System (EOSDIS) [38].

Figure 12 has more data than Figure 11 and there is one particular pixel that has an increased methane concentration. This pixel is further investigated and it is used to demonstrate how lowering the quality attribute might show something worth considering. The location of the pixel is determined in order to see if there is something that could cause the increase in methane concentration. The location of the pixel is shown in figure 14 and the pixel is circled in Figure 12.

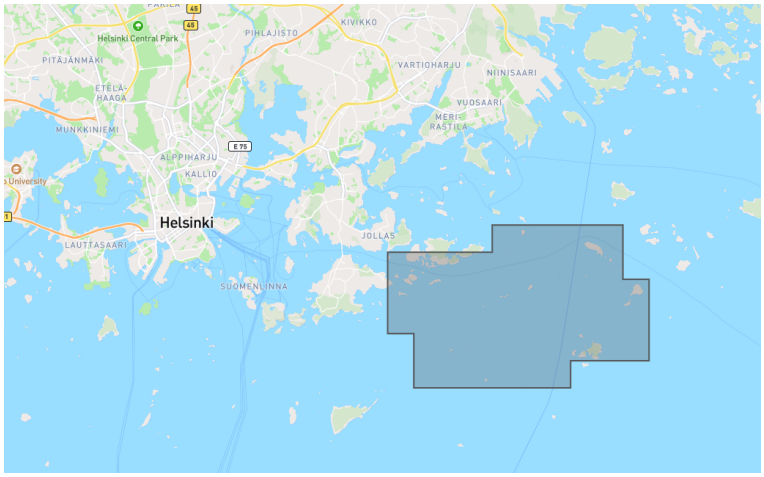

Figure 14. The location of the pixel in Finland with an enhancement of methane concentration.

In order to investigate the reliability of the pixel's increased value, methane concentration during the time of observation was also provided by the website Spectra, which is operated by the company GHGSat [41]. This website provides global information about the methane concentration over several years by combining GHGSat and TROPOMI observations. Figure 15 shows that methane concentration of the area where our pixel is seems to have increased values also according to the observations shown in Spectra.

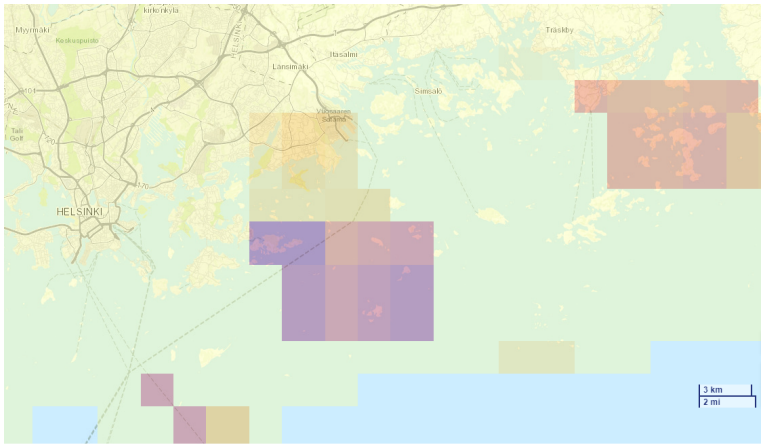

Figure 15. GHGSat's results about methane concentration during the time of observations [41].

4.3 Comparison of the areas

Figure 16 shows the distribution of XCH_4 values of the observations in Turkmenistan (31 August 2021) and Finland (17 July 2021). The y-axis shows the count of data points and x-axis shows the values of XCH_4 when quality attribute is ≥ 0.5. It is important to note that the background is not the same in both Finland and Turkmenistan. Vertical lines in Figure 16 show the median of the values at each area, i.e., where the average background methane concentration would be in each of the areas.

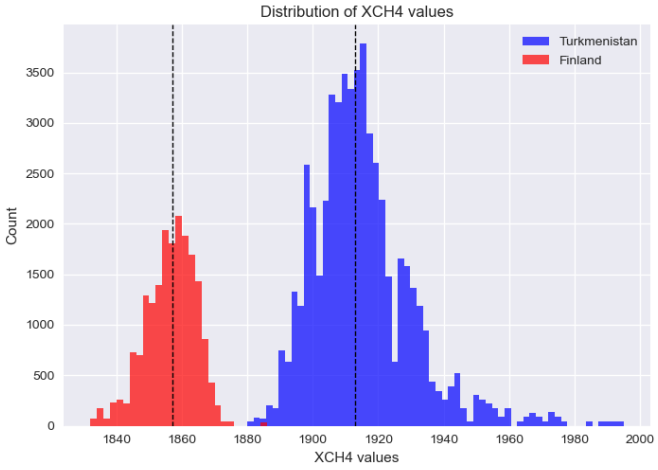

Figure 16. Distribution of XCH_4 values for both Turkmenistan and Finland. The two vertical lines represent the medians of the areas or in other words they represent the average of the background atmospheric methane. Here the quality attribute threshold is 0.5.

Figure 17 shows a similar distribution as Figure 16, but with quality attribute ≥ 0.25. The shape of Turkmenistan's distribution has not changed significantly but Finland's has and the distribution has spread to include lower values, the lowest being less than 1800 ppb. A significant increase in the count of pixels can be seen in both of the areas which was also implied in Figures 8 and 12.

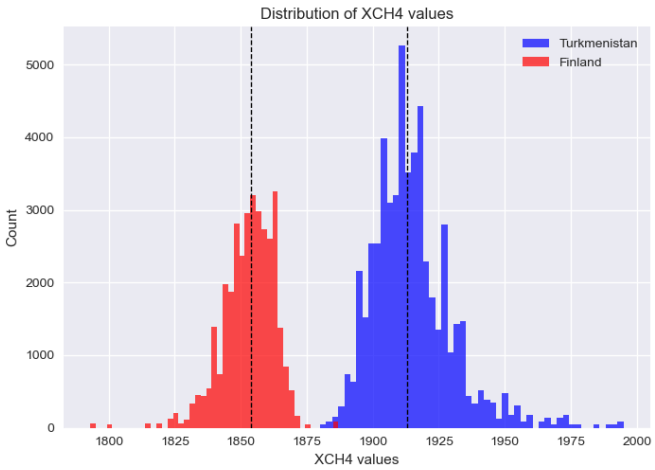

Figure 17. Distribution of XCH_4 values for both Turkmenistan and Finland with qa ≥ 0.25. The two vertical lines represent the medians of the areas.

Skewness values shown in Table I are positive for Turkmenistan, which means that the distribution is inclined to the right and so there are more higher values of methane. This is due to the two methane emission sources that were already seen in Figure 7. The skewness does not have any major difference between the different quality attributes, but with the lower quality attribute, skewness is a bit lower. This means that there are more lower methane values when the qa value is decreased.

For Finland, the skewness is negative and it changes more when the quality attribute is different. When the quality attribute is set to 0.5, skewness is closer to zero, which means that the distribution is close to Gaussian and there are no methane enhancements detected. When the quality attribute is set to 0.25, the distribution is inclined left, which means there are more lower methane concentrations, as was already seen in Figure 17.

Table I also shows the calculated medians for each distribution shown in Figures 16 and 17. The median of Turkmenistan stays the same regardless of the quality attribute, but the median of Finland decreases with a lower quality attribute, which again means that there are more lower methane values with a lower attribute.

Table I. Medians of the areas and skewness of each distribution with qa ≥ 0.5 and qa ≥ 0.25

Location	Quality attribute	Median	Skewness
Turkmenistan	0.5	1913.0	1.304
Turkmenistan	0.25	1913.0	1.287
Finland	0.5	1857.0	-0.369
Finland	0.25	1854.0	-1.013

Figure 18 shows the fraction of valid data pixels during the summer months of 2021 in both areas of interest when the quality attribute was set to 0.5. The total coverage in June, July and August 2021 is 57% in Turkmenistan and in Finland the coverage for the same period is 2%. When Figure 18 is inspected more closely, there is a significant difference between the two areas. In Turkmenistan the proportion of valid data points per day goes as high as 0.9 at best and there are several data points at that height, whereas in Finland the highest proportion of valid data points we get is only 0.4. While in Finland the amount of valid data is often zero, in Turkmenistan there are only a couple of days when this happens. In Turkmenistan the amount of valid data points seems to increase towards the end of the summer but in Finland there is most data available from 15 June to 15 July.

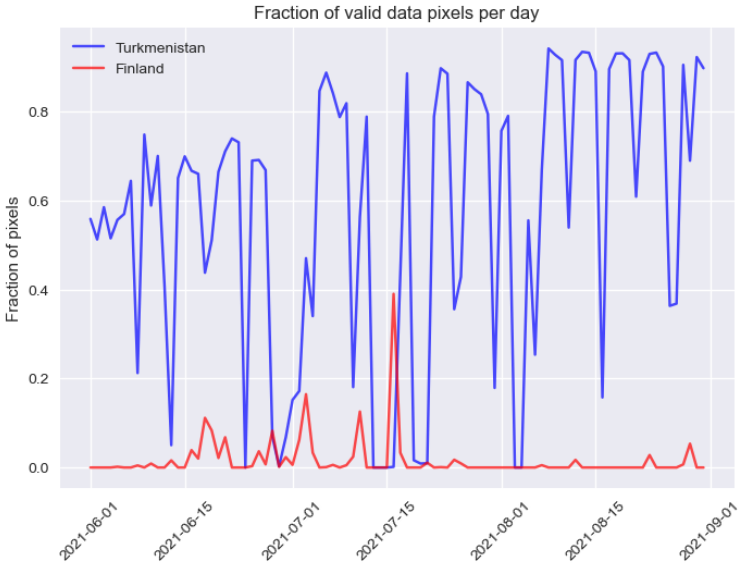

Figure 18. Fraction of valid pixels per day during the summer months in both of the areas, where the variation in the fraction of valid pixels can be seen clearly. Here quality attribute is ≥ 0.5.

Figure 19 is similar to Figure 18, but in this case quality attribute is ≥ 0.25. Figure 19 has a much higher amount of valid data points and there are very few days where the fraction of good data pixels is zero in Turkmenistan. There are still some days in Finland where the fraction is zero, but significantly less than with the higher quality attribute and there are even some days when the coverage is as good as in Turkmenistan. The total coverage in Turkmenistan is 74% and 10% in Finland and it is noted that the coverage is better in Turkmenistan than in Finland using both of the quality attributes. This implies that there is more data available for the area of interest in Turkmenistan.

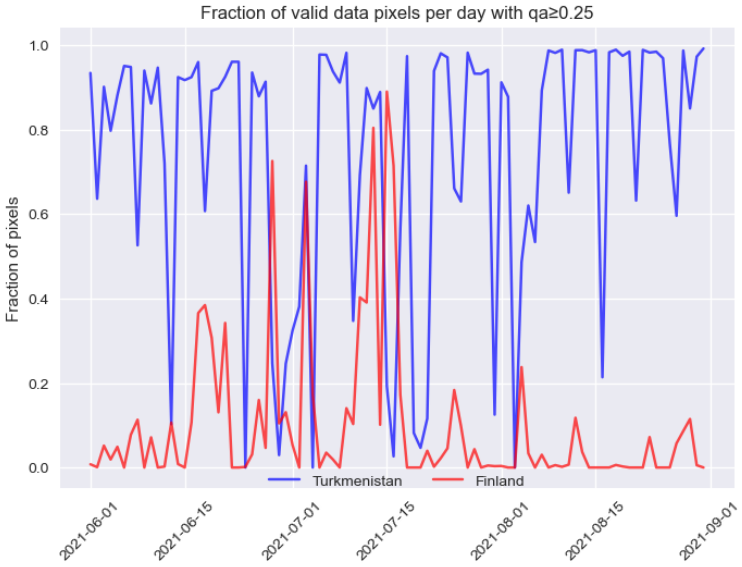

Figure 19. Fraction of valid pixels per day during the summer months in both of the areas with qa ≥ 0.25.

5 Discussion

The above results of the data analysis are compared and discussed in this Section. The idea is to see how much the area of interest affects the results that we get from TROPOMI, so a closer inspection and comparison of results is required in order to see what can be concluded about the Figures that we have.

5.1 The enhancements in Turkmenistan

The two methane enhancements seem to be spreading in certain directions in Figure 7. Figure 10 suggests that the wind at the western methane enhancement is too weak and misdirected for it to cause the spreading of the plume. According to Figure 10, the wind could be causing the spreading on the eastern enhancement since there is some spreading to the direction of the wind. However, the plume is also spread to the opposite direction and the wind cannot cause this so it is unlikely that it had a major effect on the spread.

The wind data did not explain the shape of the plumes, but there could be another explanation. The area of interest in Turkmenistan is composed of several natural gas fields. Those areas can be seen in Figure 20 in which "x" marks the areas where the two enhancements we found are located. If these enhancements are not originated from point sources, their shape cannot be directly explained by the wind. It is thus assumed that the enhancements might not be caused by just two sources, which could be the reason for their shape.

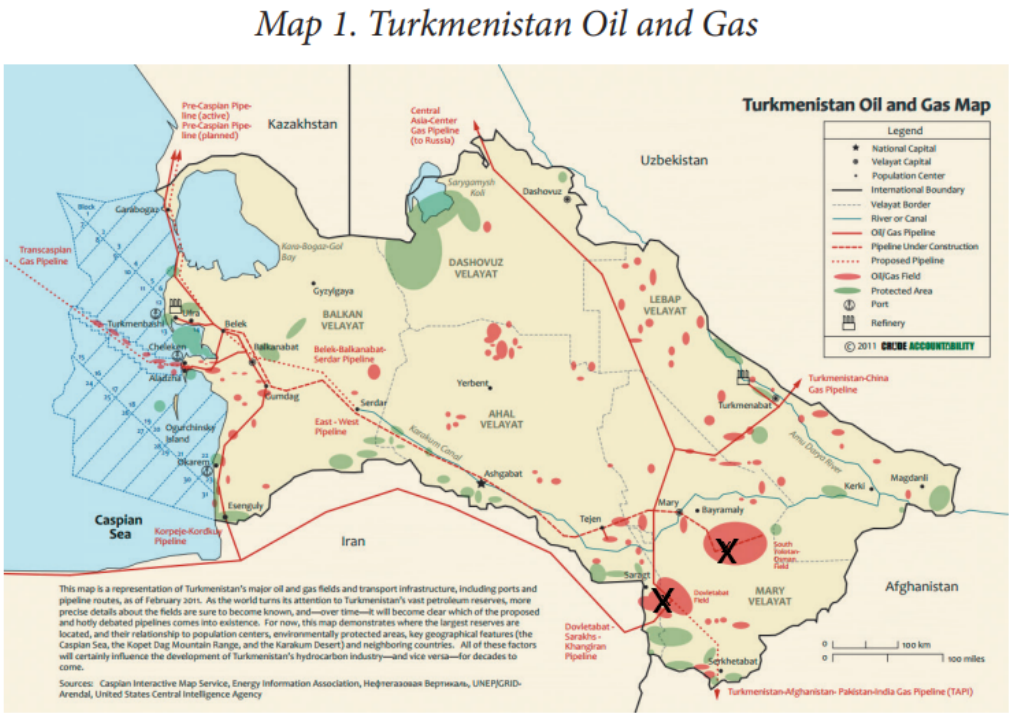

Figure 20. A map of the gas fields in Turkmenistan, where the two enhancements that we encountered are located in the areas marked with "x". [42]

5.2 The effect of the quality attribute in Finland

It was found that in Figure 12 there is one particular pixel that has a higher methane concentration compared to the other pixels. The location of the pixel is shown on a map in Figure 14 and it is noted that the pixel is in fact South of a harbour in

Vuosaari and at sea. This leaves it under the consideration of whether the increased concentration is caused by ships or if it is just an error caused by the dark surface of the water. However, according to another data source (see Figure 15), there was an increase in methane concentration at that area during the time of the observations, which could indicate that the pixel we observed with TROPOMI provides correct information and there is in fact something that causes the increased concentration. It would require broader analysis on a larger time scale and preferably validation measurements to determine the source of the enhancement and it could still turn out that it is just a coincidence. It is also important to keep in mind that the lowered quality attribute can cause problems: because these pixels are not as good quality, the results might not be as reliable and should be considered with a certain care for the application in question. Reducing the quality attribute can have benefits and it might show some interesting results, but in this case, we cannot be sure of the reliability of the pixel and reducing the quality attribute should be considered individually for each situation.

Figure 11 shows that even though there is quite a lot of missing data in Finland, in light of the fact that the natural gas fields in Turkmenistan are some of the largest anthropogenic methane emission sources, it is safe to make the assumption that there is no such methane source at the chosen area in Finland that would be major on a global scale. This assumption is also confirmed by Figure 16, where it was noted that Turkmenistan's distribution is larger and spreads on the right hand side, whereas Finland has quite an even distribution with no significant variation in values. There is seemingly one outlier in Finland's distribution, which is the previously discussed pixel. In Figure 11 these higher values can be seen as light green pixels amongst the variety of blue ones.

5.3 Comparison of the areas based on statistical analysis

From Figure 16 one can see that the two distributions are only slightly overlapping, but otherwise they have very different scales of methane and their medians are also very different. This implies that methane concentration is not constant in the atmosphere but varies depending on the area of interest.

According to Table I, the quality attribute does not have a large effect on the median at Turkmenistan as it stays the same, but in Finland there is a slight change in the median. The lower median in Finland when qa ≥ 0.25 means that there are more lower methane values taken into account when the quality of the dataset is not as good as before.

The skewness of Turkmenistan is lower with a lower quality attribute, which means that more pixels are taken into account that belong to the background. In Finland the skewness is also lower but in this case it could mean that the values that are taken into account are so low quality that their methane concentration is lower than it should be. Several results suggest that the value of the quality attribute makes a greater difference in Finland than in Turkmenistan, which means that there are possibly more contaminated pixels in Finland and the area is thus more difficult to reliably detect by TROPOMI.

There are lakes in both of the areas of interest, but in Finland there is more of them, and a major part of the missing and contaminated pixels in Figure 12 could actually be caused by lakes. These lakes are probably also the reason why the quality attribute has such a significant effect on the coverage of the area. While there are clearly two lakes that are seen in Figure 9 that most likely contaminate the pixels in Turkmenistan, not all of the water areas cause missing pixels, for example rivers that cover so little area of the pixel that there is not a large effect on the retrieval.

6 Conclusions

In this thesis we first covered the background for methane and the instrumentation used to measure its concentration. The main characteristics of CH_4 as a greenhouse gas and its detection were described, after which the S5P satellite and TROPOMI were introduced. A brief introduction was given about the retrieval algorithm that is used in retrieving TROPOMI data. The areas of interest were presented and the data analysis and methods were introduced. Finally the results were shown and discussed in more detail.

The data analysis was successful and the goal of the thesis was reached: The areas of interest were chosen well, so that the comparison was successful as the areas were very distinct and differences between them from a methane detection point of view were clear. During the data analysis we found some interesting results that were later inspected more closely using other methods, which broadened the view of the thesis and gave some insight and support to some of the more uncertain results.

Two methane enhancements were detected in Turkmenistan and the area turned out be a great example of how well methane can be detected from space when the instrument and area are well-suited. These two enhancements were used for automating the process of finding enhancements large enough for emission estimation by taking the 0.98 quantile of observations and turning them into a GeoJSON file, so that they could be saved and transported in a more compact way. The area in Finland offered a bit more of a challenge and some adjustments had to be done in order to get a better idea about methane concentration in Finland. Finland did not have any major methane enhancements when compared to Turkmenistan. However, in Finland's case, when the quality attribute was set lower there was one interesting pixel that had a higher value of methane, but the reliability and the cause of the increased concentration of that pixel remained an open question. It is clear that TROPOMI is a great instrument for detecting methane enhancements in areas such

as Turkmenistan and whilst they could also be detected in Finland using TROPOMI data, the circumstances need to be favourable and the emissions sufficiently large. The scale also has to be kept in mind since it is highly unlikely to find any huge sources on a global scale and it is likely that there is a more efficient way of detecting methane in Finland.

References

[1] O. Schneising, M. Buchwitz, M. Reuter, S. Vanselow, H. Bovensmann, and J. P. Burrows, "Remote sensing of methane leakage from natural gas and petroleum systems revisited," *Atmospheric Chemistry and Physics*, vol. 20, pp. 9169–9182, 2020.

[2] M. Pathak, R. Slade, P. Shukla, J. Skea, R. Pichs-Madruga, and D. Ürge Vorsatz, "Technical summary," 2022.

[3] D. S. Reay, P. Smith, T. R. Christensen, R. H. James, and H. Clark, "Methane and global environmental change," *Annual Review of Environment and Resources*, 6 2018.

[4] M. Cain, S. Jenkins, M. R. Allen, J. Lynch, D. J. Frame, A. H. Macey, and G. P. Peters, "Methane and the paris agreement temperature goals," 2021.

[5] P. Shukla, J. Skea, R. Slade, A. A. Khourdajie, R. van Diemen, D. McCollum, M. Pathak, S. Some, P. Vyas, R. Fradera, M. Belkacemi, A. Hasija, G. Lisboa, S. Luz, J. Malley, and (eds.), "Summary for policymakers," 2022.

[6] O. Hasekamp, A. Lorente, H. Hu, A. Butz, J. A. D. Brugh, and J. Landgraf, "Algorithm theoretical baseline document for sentinel-5 precursor methane retrieval," 2022.

[7] O. Schneising, M. Buchwitz, M. Reuter, H. Bovensmann, J. P. Burrows, T. Borsdorff, N. M. Deutscher, D. G. Feist, D. W. Griffith, F. Hase, C. Hermans, L. T. Iraci, R. Kivi, J. Landgraf, I. Morino, J. Notholt, C. Petri, D. F. Pollard, S. Roche, K. Shiomi, K. Strong, R. Sussmann, V. A. Velazco, T. Warneke, and D. Wunch, "A scientific algorithm to simultaneously retrieve carbon monoxide and methane from tropomi onboard sentinel-5 precursor," *Atmospheric Measurement Techniques*, vol. 12, pp. 6771–6802, 2019.

[8] D. J. Wuebbles and K. Hayhoe, "Atmospheric methane and global change," 2001.

[9] T. Lauvaux, C. Giron, M. Mazzolini, A. D'Aspremont, R. Duren, D. Cusworth, D. Shindell, and P. Ciais, "Global assessment of oil and gas methane ultra-emitters," *Science*, vol. 375, 2022.

[10] X. Lan, K. Thoning, and E. Dlugokencky, "Trends in globally-averaged ch4, n2o, and sf6 determined from noaa global monitoring laboratory measurements." https://gml.noaa.gov/ccgg/trends_ch4/, 2.5.2023.

[11] J. Hachmeister, O. Schneising, M. Buchwitz, A. Lorente, T. Borsdorff, J. P. Burrows, J. Notholt, and M. Buschmann, "On the influence of underlying elevation data on sentinel-5 precursor tropomi satellite methane retrievals over greenland," *Atmospheric Measurement Techniques*, vol. 15, pp. 4063–4074, 7 2022.

[12] J. A. de Gouw, J. P. Veefkind, E. Roosenbrand, B. Dix, J. C. Lin, J. Landgraf, and P. F. Levelt, "Daily satellite observations of methane from oil and gas production regions in the united states," *Scientific Reports*, vol. 10, pp. 1–10, 2020.

[13] P.Huhtanen, E. Cabezas-Garcia, S. Utsumi, and S. Zimmerman, "Comparison of methods to determine methane emissions from dairy cows in farm conditions," 2015.

[14] R. Parker, H. Boesch, A. Cogan, A. Fraser, L. Feng, P. I. Palmer, J. Messerschmidt, N. Deutscher, D. W. Griffith, J. Notholt, P. O. Wennberg, and D. Wunch, "Methane observations from the greenhouse gases observing satellite: Comparison to ground-based tccon data and model calculations," *Geophysical Research Letters*, vol. 38, 8 2011.

[15] S. E. Reutebuch, "Light detection and ranging (lidar): An emerging tool for multiple resource inventory biophysical controls on forest structure and fire severity in yosemite national park view project," 2005.

[16] A. P. Ravikumar, J. Wang, and A. R. Brandt, "Are optical gas imaging technologies effective for methane leak detection?," *Environmental Science and Technology*, vol. 51, pp. 718–724, 1 2017.

[17] J. Mellqvist, J. Samuelsson, J. Johansson, C. Rivera, B. Lefer, S. Alvarez, and J. Jolly, "Measurements of industrial emissions of alkenes in texas using the solar occultation flux method," *Journal of Geophysical Research: Atmospheres*, vol. 115, 2010.

[18] "Long open-path laser dispersion sensing." https://www.ralspace.stfc.ac.uk/Pages/Long-open-path-laser-dispersion-sensing.aspx. Accessed: 6.3.2023.

[19] H. Rottländer, W. Umrath, and G. Voss, "Fundamentals of leak detection," 2016.

[20] H. Lua, T. Iseley, S. Behbahani, and L. Fu, "Leakage detection techniques for oil and gas pipelines: State-of-the-art," 2019.

[21] H. Hu, O. Hasekamp, A. Butz, A. Galli, J. Landgraf, J. A. D. Brugh, T. Borsdorff, R. Scheepmaker, and I. Aben, "The operational methane retrieval algorithm for tropomi," *Atmospheric Measurement Techniques*, vol. 9, pp. 5423–5440, 2016.

[22] D. J. Varon, J. McKeever, D. Jervis, J. D. Maasakkers, S. Pandey, S. Houweling, I. Aben, T. Scarpelli, and D. J. Jacob, "Satellite discovery of anomalously large methane point sources from oil/gas production," *Geophysical Research Letters*, vol. 46, pp. 13507–13516, 11 2019.

[23] A. Apituley, M. Pedergnana, M. Sneep, J. Pepijn, D. Loyola, O. Hasekamp, A. L. Delgado, and T. Borsdorff, "Sentinel-5 precursor/tropomi level 2 product user manual methane document number : Sron-s5p-lev2-ma-001," 2022.

[24] H. Suto, F. Kataoka, N. Kikuchi, R. O. Knuteson, A. Butz, M. Haun, H. Buijs, K. Shiomi, H. Imai, and A. Kuze, "Thermal and near-infrared sensor for carbon observation fourier transform spectrometer-2 (tanso-fts-2) on the greenhouse gases observing satellite-2 (gosat-2) during its first year in orbit," *Atmospheric Measurement Techniques*, vol. 14, pp. 2013–2039, 3 2021.

[25] "Smarter data for a stronger planet." https://kuvaspace.com/. Accessed: 2.5.2023.

[26] "Methane alert and response system (mars)." https://www.unep.org/explore-topics/energy/what-we-do/methane/imeo-action/methane-alert-and-response-system-mars. Accessed: 4.2023.

[27] "Bridging the gap." https://www.methanesat.org/satellite/. Accessed: 2023.

[28] "Satellite missions catalogue." https://www.eoportal.org/satellite-missions/. Accessed: 10.5.2023.

[29] E. Sánchez-García, J. Gorroño, I. Irakulis-Loitxate, D. J. Varon, and L. Guanter, "Mapping methane plumes at very high spatial resolution with the worldview-3 satellite," 2022.

[30] H. Hu, J. Landgraf, R. Detmers, T. Borsdorff, J. A. de Brugh, I. Aben, A. Butz, and O. Hasekamp, "Toward global mapping of methane with tropomi: First results and intersatellite comparison to gosat," *Geophysical Research Letters*, vol. 45, pp. 3682–3689, 2018.

[31] T. Lauvaux, C. Giron, M. Mazzolini, A. D'Aspremont, R. Duren, D. Cusworth, D. Shindell, and P. Ciais, "Global assessment of oil and gas methane ultra-emitters," *Science*, vol. 375, pp. 557–561, 2022.

[32] J. Landgraf, A. Lorente, B. Langerock, M. K. Sha, J. c Lambert, D. Loyola, and D. S. Zweers, "S5p mission performance centre methane l_2ch_4 readme document number issue 2.2 date prepared by reviewed by," 2022.

[33] "What is swir?." https://www.edmundoptics.com/knowledge-center/application-notes/imaging/what-is-swir/. Accessed: 9.5.2023.

[34] A. Lorente, T. Borsdorff, A. Butz, O. Hasekamp, J. A. D. Brugh, A. Schneider, L. Wu, F. Hase, R. Kivi, D. Wunch, D. F. Pollard, K. Shiomi, N. M. Deutscher, V. A. Velazco, C. M. Roehl, P. O. Wennberg, T. Warneke, and J. Landgraf, "Methane retrieved from tropomi: Improvement of the data product and validation of the first 2 years of measurements," *Atmospheric Measurement Techniques*, vol. 14, pp. 665–684, 2021.

[35] S. Pandey, S. Houweling, A. Lorente, T. Borsdorff, M. Tsivlidou, A. Bloom, B. Poulter, Z. Zhang, and I. Aben, "Using satellite data to identify the methane emission controls of south sudan's wetlands," 2020.

[36] J. T. Shaw, A. Shah, H. Yong, and G. Allen, "Methods for quantifying methane emissions using un manned aerial vehicles: a review," 2021.

[37] "Gas transmission network." https://gasgrid.fi/en/gas-network/gas-transmission-network/. Accessed: 6.3.2023.

[38] "Worldview." https://worldview.earthdata.nasa.gov/. Accessed: 2.5.2023.

[39] "Era5 hourly data on single levels from 1940 to present." https://cds.climate.copernicus.eu/cdsapp#!/dataset/reanalysis-era5-single-levels?tab=form. Accessed: 3.3.2023.

[40] D. Zwillinger and S. Kokoska, "Crc standard probability and statistics tables and formulae," 2000.

[41] "Spectra." https://spectra-basic.ghgsat.com/. Accessed: 11.5.2023.

[42] M. Laruelle and N. Muradova, "Turkmenistan: Changes and stability under berdimuhamedow," *Atmospheric Measurement Techniques*, p. 10, 2015.